Thermal properties and crystal structures of manganese(III)-salen complexes with the Tf2N anion [Tf2N =bis(trifluoromethanesulfonyl)amide)]

Okuhata, Megumi

Mochida, Tomoyuki

(Citation)
Polyhedron,43(1):153-158

(Issue Date)
2012-08-13

(Resource Type)
journal article

(Version)
Accepted Manuscript

(URL)
https://hdl.handle.net/20.500.14094/90001814

Thermal properties and crystal structures of manganese(III)–salen complexes with the Tf_2N anion [Tf_2N = bis (trifluoromethanesulfonyl)amide)]

Megumi Okuhata, Tomoyuki Mochida*

Department of Chemistry, Graduate School of Science, Kobe University, Rokkodai, Nada, Hyogo 657-8501, Japan

ABSTRACT

A series of salts comprising cationic manganese(III)–salen complexes and the Tf_2N anion has been prepared (salen = *N*,*N*′-bis(salicylideneaminato)ethylene, Tf_2N = bis(trifluoromethanesulfonyl)amide) to investigate the effects of axial ligands and substituents on their thermal properties. [Mn(salen)L_2][Tf_2N] (L = H_2O, Pyridine) and their 5–butoxysalen analogues undergo thermal desorption of the axial ligands, followed by decomposition above 250°C. The pyridine complexes exhibit two-step ligand desorption, corresponding to the formation of a dimer and later, desorption from the dimer. Complexes with L = 3-butylpyridine and *N*-butylimidazole melt at 97.6°C and 132.7°C, respectively, before ligand desorption. Crystal structures of these and related complexes have been determined. [Mn(salen)(3,3′-bipyridine)][Tf_2N] is a coordination polymer with higher thermal stability.

Keywords: Salen complex, Manganese, Axial ligand, Thermal analysis, Crystal structure

---

*Corresponding author. Tel/fax: +81-78-803-5679, *E-mail address:* tmochida@platinum.kobe-u.ac.jp (T. Mochida).

1. Introduction

N, *N*′-Bis(salicylideneaminato)ethylene (= salen) is a chelate ligand with a rich coordination chemistry that has produced many versatile metal complexes [1]. In particular, manganese(III) salen complexes have attracted interest in diverse areas such as catalysts [2], models of active centers of metalloenzymes and proteins [3], and as molecular magnets [4].

We have recently prepared ionic liquids comprising organometallic cations and bis(trifluoromethanesulfonyl)amide (= Tf_2N) [5]. Ionic liquids are salts with melting points below 100°C, and they have recently attracted much attention for both basic science and in applications [6]. Tf_2N is often used as an anion in ionic liquids because it tends to give salts with lower melting points when compared to other anions [6,7]. In this context, we are interested in the thermal properties of Tf_2N salts of cationic salen complexes. In this study, a series of manganese-salen complexes [Mn(salen)L_2][Tf_2N] (L = H_2O (**1a**), pyridine (**1b**), 3-butylpyridine (**1c**), *N*-butylimidazole (**1d**)), [Mn(5-butoxysalen)L_2][Tf_2N] (L = H_2O (**2a**), pyridine (**2b**)) (Chart 1) were prepared to investigate the effect of axial ligands and substituents on their thermal properties. The crystal structures of **1a**, [Mn_2(salen)$_2$(H_2O)$_2$][Mn(salen)(H_2O)$_2$][Tf_2N]$_3$ (**1a′**), [Mn_2(salen)$_2$(*N*-butylimidazole)$_2$][Tf_2N]$_2$ (**1d′**), and [Mn(salen)(3,3'-bipyridine)][Tf_2N] (**3**) (Chart 2) are also reported here. Previous studies have been made on the thermal decomposition behaviors of salen-type complexes [8]. Salen complexes with imidazolium moieties [9] and with alkyl chains [10] have also been reported.

2. Results and Discussion

2.1. Preparation

1a' and **2a**, which bear axial water ligands, were prepared by reacting the corresponding salen ligands with manganese acetate in ethanol, followed by anion exchange and recrystallization from acetone. **1a** was obtained similarly from acetone containing a small amount of water. Compounds with *N*-donor axial ligands, **1b**–**d**, **2b**, and **3**, were prepared by adding the corresponding axial ligands to solutions of either **1a** or **2a**, followed by recrystallization. **1d′** was a dimer complex obtained in a very small yield from the same reaction as **1d**. The formation of both complexes is ascribed to an equilibrium of the monomer and dimer in solution [3].

2.2. Thermal properties

1c and **1d** exhibited melting points, whereas the remainder of the complexes exhibited only decomposition. The melting point of the butylpyridine complex **1c** (T_m = 97.6°C) was lower than that of the butylimidazole complex **1d (**T_m = 132.7°C). Differential scanning calorimetry (DSC) traces of **1c** and **1d** are shown in Fig. 1. **1c** exhibited a somewhat broad melting peak at 97.6°C (ΔH = 45.2 kJ mol^{-1}, ΔS = 119.7 $JK^{-1}mol^{-1}$). Crystallization occurred at 73°C upon cooling from the melt. With repeating the cycles, the melting peak gradually shifted to lower temperatures, accompanying by a decrease in peak area. This has been ascribed to gradual desorption of the axial ligand (*vide infra*). **1d** exhibited a sharp melting peak at 132.7°C (ΔH = 58.1 kJ mol^{-1}, ΔS = 142.7 J K^{-1} mol^{-1}). When cooled from the melt, the complex exhibited a glass transition at 4 °C, and crystallization occurred in the heating process at 70°C. The melting and crystallization behavior of **1d** was reversible.

The weight loss temperatures (−3wt%) determined by thermogravimetric (TG) analysis for **1c** and **1d** are 106°C and 156°C, respectively. The weight loss corresponds to the desorption of the axial ligands. The axial ligand in **1c** starts desorption near the melting point, whereas **1d** is stable after melting. The lower desorption temperature of **1c** is ascribed to the weaker coordination ability of pyridine than imidazole [10]. TG traces of these salts are shown in Fig. 2a. The TG trace of **1c** decreases in several steps, and the loss from 90–270°C (30.8%) corresponds to the complete desorption of the axial ligand (calc. 31.0%). In **1d**, the weight loss is continuous and desorption of the axial ligand and decomposition were not discriminated.

The other mononuclear complexes (**1a**–**b**, **2a**–**b**) decomposed without melting, after desorption of the axial ligands. Their TG traces are shown in Fig. 2b. **1a** exhibited a weight loss between 100−130°C (−3.3%), which correspond to the loss of the axial water molecules (calc. −2.9wt%), and weight loss at 307°C (−3wt%) is due to decomposition. In **1b** and **2b**, desorption of the pyridine axial ligands occurred in two steps. This feature suggests that a dimer is formed in the first step by desorption of one of the two axial ligands and the desorption of the axial ligands from the dimer complex occurs in the second step. The weight loss of **1b** occurred from 75–125°C (−9.9%) and from 130–180°C

(−9.5%), the sum of which corresponds to the loss of both pyridines (calc. −20.8%). Similarly, the weight loss in **2b** occurred from 90–115°C (−8.9%) and from 125–180°C (−8.4%), the sum of which corresponds to the calculated value (calc. −17.5%) for the loss of the pyridines. The decomposition temperatures (–3wt%) of the now ligand free forms of **1b** and **2b** are 293°C and 285°C, respectively. The weight loss temperature (–3 wt%) of the coordination polymer **3** was 250°C, which suggests that the bridging ligand in **3** is, as expected, more tightly held than those in other mononuclear complexes.

As shown above, the compounds with axial ligands of pyridine or water do not exhibit melting even when a butoxy group is introduced into the salen ligand. These axial ligands easily dissociate on heating. The resultant axial ligand-free complexes are probably joined by Mn...O bonds that are seen in the salen dimers, as suggested by the stepwise ligand desorption behavior seen in the pyridine complexes. Thus these complexes do not melt and only decompose at high temperatures. In contrast, introducing an alkyl group into the axial ligand leads to melting. This is ascribed to the higher ligand desorption temperatures as well as to the lowering of the melting points due to the flexibility of the alkyl group. However, the melting points of these salts are not low enough to be regarded as room-temperature ionic liquids, although there are butylimidazole-coordinated metal complexes that exhibit low melting points [12]. The high melting points of the present salts are probably ascribed to the high planarity and high symmetry of the unit.

*2.3. Crystal structures of **1a** and **1a′***

1a and **1a′** crystallized in the space group *P*−1. The molecular structure of the cation and the packing diagram of **1a** are shown in Fig. 3. The salen ligand is slightly twisted out of planarity. The Tf_2N anion adopts the *cis* conformation. The hydrogen atoms of the axial water are hydrogen-bonded to an oxygen of the neighboring salen unit or an oxygen in the SO_2 group of Tf_2N (Fig. 3b). Hydrogen bond distances of the former (O…O distances: 2.73–2.75 Å) are shorter than those of the latter (2.83–3.03 Å). There are two hydrogen bonds between the neighboring salen units, which link the cations to form one-dimensional hydrogen-bonded chains along the *a*-axis. The chains are further bridged by Tf_2N via hydrogen bonds.

1a′ contains two types of cation, a monomer and a phenoxo-bridged dimer in a ratio of 1:1. The

structure of the dimer and the packing diagram of **1a′** are shown in Fig. 4. The Mn…Mn separation in the dimer is 3.325(1) Å. Tf_2N again adopts the *cis* conformation. Intermolecular hydrogen bonds similar to **1a** are formed, by which two dimers and two monomers are linked alternately along [101] to form a one-dimensional chain structure (Fig. 4b), which are further bridged by Tf_2N. The overall molecular arrangement is similar to that of **1a**; hence, these salts may be regarded as pseudo supramolecular isomers.

The hydrogen-bonded network structures observed in **1a** and **1a′** are seen in other Schiff-base manganese complexes with water axial ligands [13], such as monomer complexes $[M(salen)(H_2O)_2]X$ (M = Cr, Co, Mn) [14] and the dimer complex $[Mn_2(salen)_2(H_2O)_2][ClO_4]_2$ [15]. The coexistence of the monomer and dimer is seen in $[Mn(5\text{-}Brsalen)_2(H_2O)_2][Mn(5\text{-}Brsalen)(H_2O)_2]_2[ClO_4]_4\cdot 4H_2O$ [16] and a related Schiff-base complex [17]. Concerning magnetic properties, mononuclear salen salts usually exhibit negligible or very small antiferromagnetic interactions [14]. Dimeric salen manganese complexes generally exhibit antiferromagnetic intradimer interactions, whereas some complexes show very small ferromagnetic interactions [4,15]. **1a** and **1a′** may exhibit similar magnetic behaviors.

*2.4. Crystal structure of **1d′***

The packing diagram of **1d′** is depicted in Fig. 5. This salt crystallized in the space group *P*–1. There are two crystallographically independent dimers (dimer I and II, Fig. 5), and both are centrosymmetric. Two *N*-butylimidazole molecules are coordinated as axial ligands, and the butyl groups in dimer II are disordered. Tf_2N adopts the *cis* conformation. The N…Mn coordination distances for dimer I and dimer II are 2.228(2) Å and 2.213(2) Å, respectively. Dimer I is stacked one-dimensionally along the *a*-axis through π–π interactions between the benzene moieties, with their molecular planes inclined. Dimer II exhibits no such π–π interactions.

*2.5. Crystal structure of **3***

The crystal structure of **3** is shown Fig. 6. The space group is *C2/c*, and there is one crystallographically independent salen and 3,3′-bipyridine per unit cell. This complex is a coordination

polymer, in which the bipyridine bridges the salen units, forming one-dimensional linear chains extending along [110] and [1−10]. The N…Mn coordination distances are 2.349(2) Å and 2.372(2) Å. The two pyridine rings in 3,3′-bipyridine are at 37.1(2)° with respect to each other. Tf_2N adopts the *trans* conformation. Related examples of salen-bases coordination polymers bridged by pyridine analogs are known, such as [Fe(salen)(4,4′-azopyridine)][BPh_4] [18]. There are also hydrogen-bonded chain complexes such as [Fe(salen)(4,4′-bipyridine)(MeOH)][BPh_4] [18].

3. Conclusion

A series of Tf_2N salts of cationic manganese(III)–salen complexes have been prepared and their thermal properties investigated. Starting from [Mn(salen)(H_2O)$_2$][Tf_2N], the effects of introducing butoxy groups onto the salen and changing the axial ligands has been examined. The salts with axial ligands of water or pyridine decompose at high temperatures which involves the desorption of the ligands. However, the salts with axial ligands of 3-butylpyridine or *N*-butylimidazole exhibit melting near or above 100°C. The lowering of the melting points is ascribed to less easy desorption of the alkylated ligands and the flexibility of the alkyl groups. Thermal stability and reversibility of the melting and crystallization behavior are high for the complex with butylimidazole.

This study has revealed the role of the axial ligands on the thermal behaviors of manganese(III)-salen salts. The results suggest that salts with such planar metal complexes exhibit high melting points despite the use of Tf_2N and introduction of alkyl groups. The use of other cationic Schiff base complexes, producing room temperature ionic liquids, will be reported elsewhere [19].

4. Experimental

4.1. General

[Mn(salen)][CH_3COO] and 2-hydroxy-5-butoxybenzaldehyde were prepared according to literature methods [20,21]. Other reagents and solvents were obtained commercially. ^{1}H NMR spectra were recorded on a JEOL JNM-ECL-400 spectrometer. Infrared spectra were recorded on a Thermo Nicolet Avatar 360 spectrometer as KBr pellets or on a Thermo Nicolet iS5 spectrometer equipped with a diamond ATR unit. Elemental analyses were performed using a Yanaco CHN coder MT-5. TG

analysis was performed under a nitrogen atmosphere at a heating rate of 5 K min^{-1} on a Seiko TG/DTA 220U. DSC measurements were performed using a TA instruments Q100 differential scanning calorimeter at 10 K min^{-1} at temperatures down to 100 K.

*4.2. Preparation of **1a–d***

To a solution of [Mn(salen)][CH_3COO] (450 mg, 1.18 mmol) in 50 mL of water was added LiTf2N (384 mg, 1.33 mmol). A precipitate formed, which was collected by filtration, and purified on a short plug of alumina (eluent: ethanol). Yield 462 mg (64.9%). The product was recrystallized by a diffusion method: the compound was dissolved in acetone/ether (1:1), and ether and pentane were successively layered over the solution in a test tube and allowed to diffuse over a week. When water-containing acetone was used in the diffusion method, crystals of **1a** were formed. Anal. Calcd. For $C_{18}H_{18}N_3O_8F_6S_2Mn$: C, 33.92; H, 2.85; N: 6.59. Found: C, 34.46; H, 2.78; N, 6.75. Without adding water, a complex with a lower water content was obtained. Anal. Calcd. For $C_{36}H_{28}N_6O_{16}F_{12}S_4Mn_2$ (= $[Mn_2(salen)_2(H_2O)_2][Tf_2N]_2$): C, 34.90; H, 2.60; N: 6.78. Found: C, 35.12; H, 2.20; N, 6.83. A single crystal collected from the mixture was found to be $[Mn_2(salen)_2(H_2O)_2][Mn(salen)(H_2O)_2][Tf_2N]_3$ (**1a′**) according to X-ray crystal structure analysis.

1b was obtained as a black solid by adding pyridine (0.2 mL, 2.55 mmol) to an acetone solution of **1a** (51.6 mg, 0.086 mmol), followed by vapor diffusion with hexane. Yield 63.2 mg (97.1%). Anal. Calcd. For $C_{28}H_{24}N_5O_6F_6S_2Mn$: C, 44.27; H, 3.18; N, 9.22. Found: C, 44.87; H, 3.25; N, 9.22. **1c** was obtained as brown block crystals by the same procedure, except that 3-butylpyridine was used as the axial ligand. Yield 37.9 mg (91.6%). Anal. Calcd. For $C_{36}H_{40}N_5O_6F_6S_2Mn$: C, 49.60; H, 4.62; N, 8.03. Found: C, 49.52; H, 4.80; N, 8.28.

1d was prepared by adding **1a** (31.2 mg, 0.049 mmol) to a dichloromethane solution (1 mL) of *N*-butylimidazole (0.0185 mL, 0.141 mmol), followed by vapor diffusion of ether or hexane into this solution to give a yellowish brown powder. Yield 25.9 mg (64.7%). Anal. Calcd. For $C_{32}H_{40}N_7O_6F_6S_2Mn$: C, 45.12; H, 4.73; N, 11.51. Found: C, 45.57; H, 4.53; N, 11.58. Together with **1d**, a very small amount of black crystals of [Mn(salen)(*N*-butylimidazole)]$_2$[Tf_2N]$_2$ (**1d′**) was obtained.

We also tried to prepare a complex with triethylamine axial ligand by the same procedure. The

axial ligands, however, were found to exchange with water from the air.

*4.3. Preparation of **2a–b***

To prepare the ligand, ethylenediamine was added dropwise to a solution of 2-hydroxy-5-butoxybenzaldehyde (346 mg, 1.78 mmol) in ethanol (2 mL) at 50°C with stirring. The solution was allowed to cool to room temperature and the resulting microcrystals of 5-butoxysalen were collected by filtration, dried under vacuum, and purified by recrystallization from ethanol. Yield 201 mg (54.8%). ^{1}H NMR (400 MHz, $CDCl_3$, ppm) δ = 12.68 (s, 2H), 8.29 (s, 2H), 6.89–6.73 (m, 6H), 3.93 (s, 4H), 3.88 (t, 4H), 1.72 (t, 4H), 1.46 (q, 4H), 0.96 (t, 6H). The so prepared 5-butoxysalen (159 mg, 0.385 mmol) was dissolved in ethanol (20 mL) with heating. To this solution was added an ethanol solution of manganese acetate tetrahydrate (96.5 mg, 0.385 mmol) with stirring. The solution was evaporated, and the residue was dissolved in water (175 mL), and LiTf2N (132.6 mg, 0.462 mmol) was added with stirring. A dark green precipitate of **2a** was formed, which was collected by filtration, and purified on a short plug of alumina (eluent: ethanol). Yield 230 mg (80.1%). Single crystals were obtained by recrystallized from acetone. Anal. Calcd. For $C_{26}H_{38}N_3O_{10}F_6S_2Mn$: C, 39.95; H, 4.38; N, 5.38. Found: C, 39.94; H, 4.28; N, 5.30. **2b** was prepared as described for **1b**, using **2a** as a starting material, in a yield of 88.5%.

*4.4. Preparation of **3***

3 was obtained as black block crystals by same procedure as that of **1b**, except that 3,3'-bipyridine was used as axial ligand. Yield 33.9 mg (87.8%). Anal. Calcd. For $C_{46}H_{40}N_8O_{14}F_{12}S_4Mn_2$ (a 1:1 mixture of [Mn(salen)(bpy)][Tf_2N] and [Mn(salen)(H_2O)$_2$][Tf_2N]): C, 39.53; H, 2.89; N, 8.03. Found: C, 39.53; H, 3.08; N, 7.86. Single crystals were collected and used for measurements. IR (ATR Diamond): ν(C–H) 3066–2922, ν(C=N) 1615, ν(O=S=O) 1129 and 1290, ν(C–F) 1171, δ(C–H) 705, 739 cm^{-1}.

4.5. Crystal structure determination

X-ray diffraction data for **1a**, **1a′**, **1d′**, and **3** were collected on a Bruker SMART APEX II CCD

diffractometer using MoKα radiation (λ = 0.71073 Å) at 100 K. Crystallographic parameters are listed in Table 1. The structures were solved by direct methods and refined on F^2 using SHELX-97 [22]. Empirical absorption correction was applied (SADABS [23]). The non-hydrogen atoms were refined anisotropically. The anions in **1a'** and **3** were partly disordered, where the occupancy of the minor sites were less than 20%. ORTEP-3 [24] was used to generate the molecular graphics.

Acknowledgments

We thank Y. Funasako for his help with structure analysis, Y. Furuie for elemental analysis, and M. Nakama (Crayonsoft Inc.) for providing a web-based database. This work was supported by a Grant-in-Aid for Scientific Research (No. 21350077) from the Japan Society for the Promotion of Science (JSPS).

Appendix A. Supplementary data

CCDC 801666 (**1a**), 801667 (**1a′**), 831470 (**1d′**), and 853575 (**3**) contains the supplementary crystallographic data for this paper. These data can be obtained free of charge via http://www.ccdc.cam.ac.uk/conts/retrieving.html, or from the Cambridge Crystallographic Data Centre, 12 Union Road, Cambridge CB2 1EZ, UK; fax: (+44) 1223-336-033; or e-mail: deposit@ccdc.cam.ac.uk.

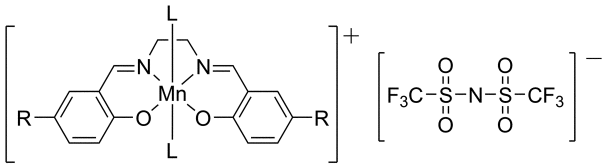

1a: R = H, L = H_2O
1b: R = H, L = pyridine
1c: R = H, L = 3-butylpyridine
1d: R = H, L = *N*-butylimidazole
2a: R = BuO, L = H_2O
2b: R = BuO, L = pyridine

Chart 1.

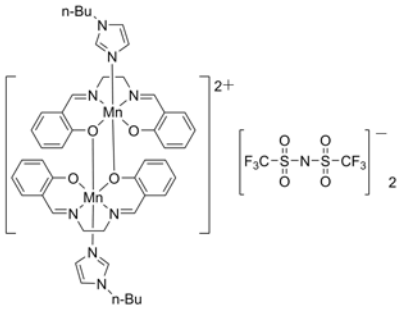

1d'

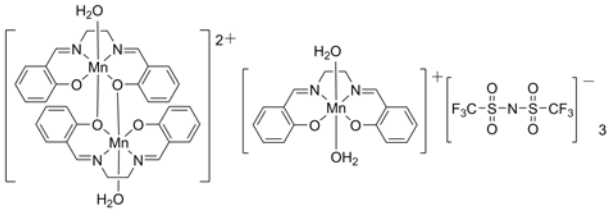

1a'

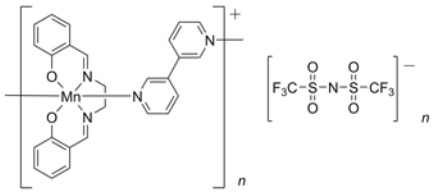

3

Chart 2.

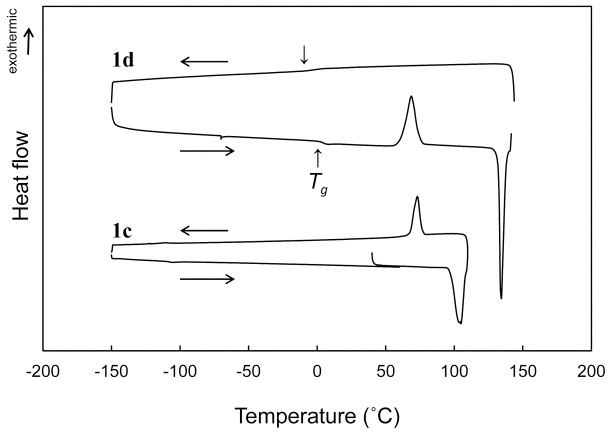

Fig. 1. DSC curves of **1c** and **1d**. A cooling–heating cycle after the first melting is shown for **1d**.

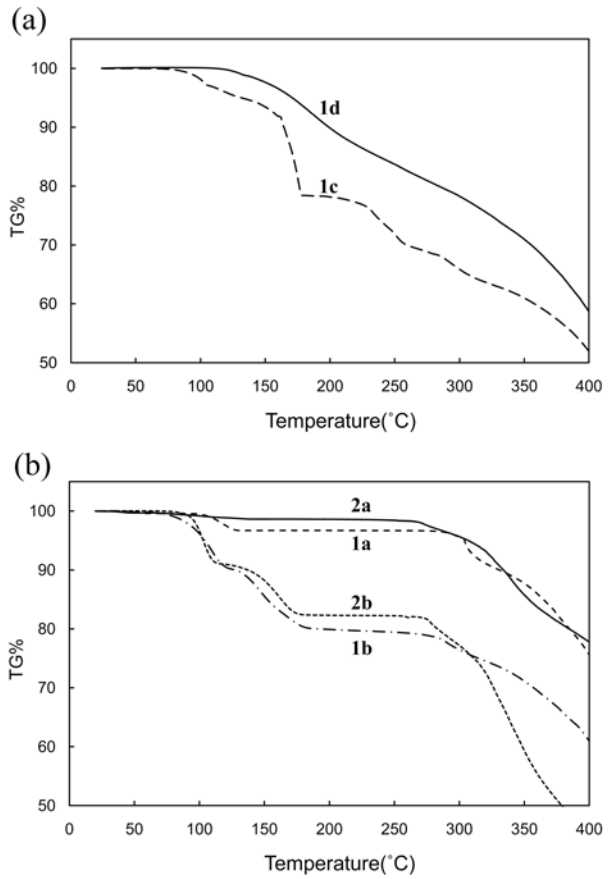

Fig. 2. Thermogravimetric traces of (a) **1c**–**d**, and (b) **1a**–**b** and **2a**–**b**.

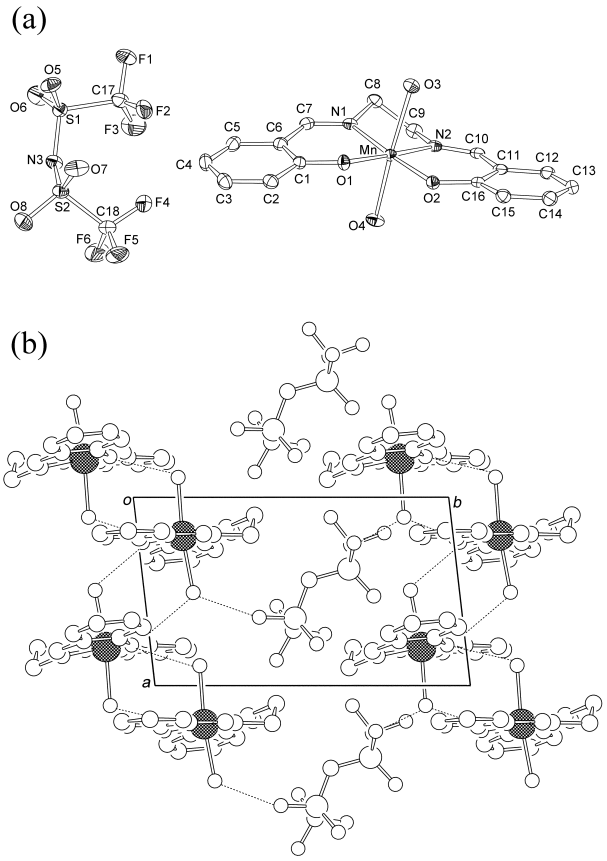

Fig. 3. Crystal structure of **1a**. ORTEP drawing of (a) the molecular structures and (b) packing diagram projected along the *c*-axis. Hydrogen bonds are represented by dashed lines. Hydrogen atoms have been omitted for clarity.

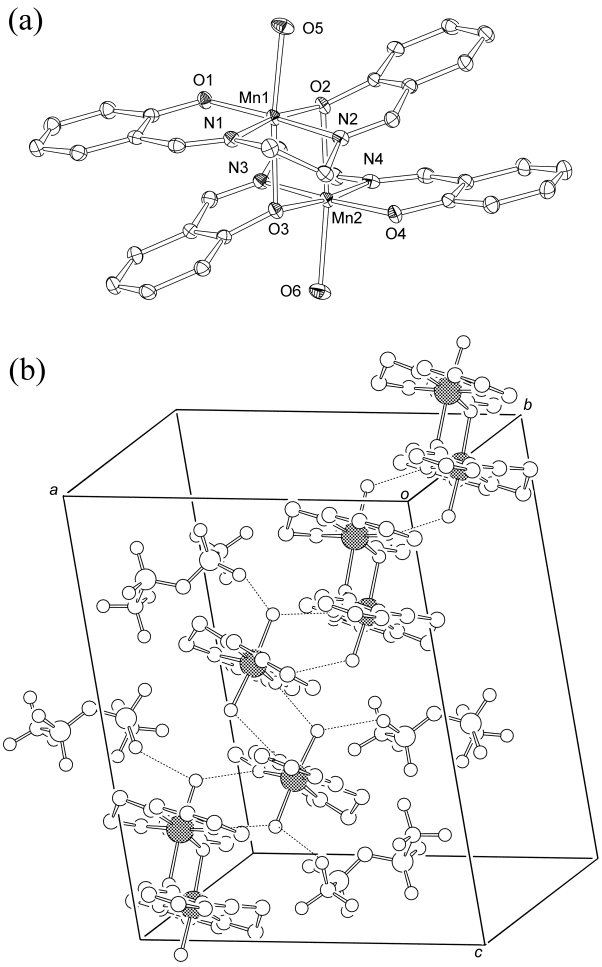

Fig. 4. Crystal structure of **1a′**. ORTEP drawing of (a) the molecular structure of the dimer unit and (b) packing diagram. Hydrogen bonds are represented by dashed lines. Hydrogen atoms have been omitted for clarity.

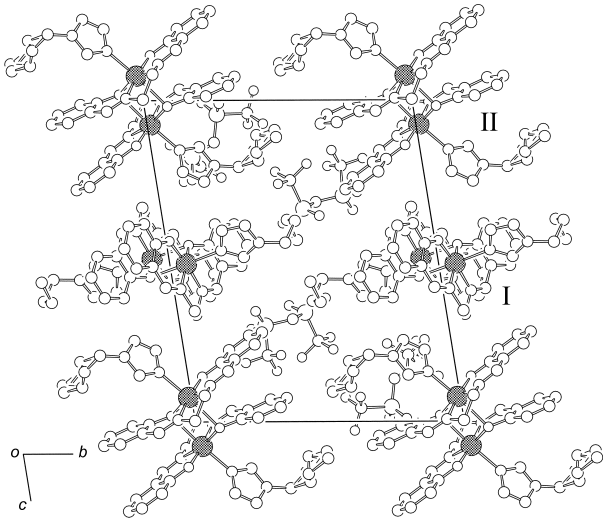

Fig. 5. Packing diagram of **1d′** viewed along the *a*-axis. Hydrogen atoms have been omitted for clarity. I and II denote crystallographically independent dimers.

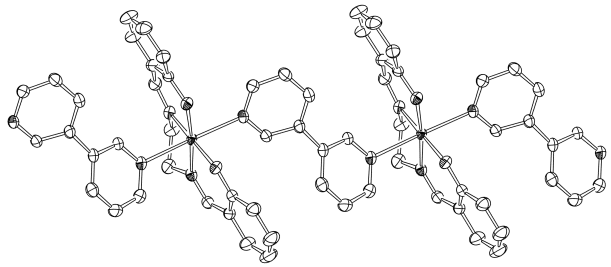

Fig. 6. ORTEP drawing of the 1-D chain structure in **3**.

Table 1

Crystallographic parameter of **1a**, **1a'**, **1d'** and **3**

	1a	**1a'**	**1d'**	**3**
Empirical formula	$C_{18}H_{18}F_6MnN_3O_8S_2$	$C_{54}H_{50}F_{18}Mn_3N_9O_{22}S_6$	$C_{50}H_{52}F_{12}Mn_2N_{10}O_{12}S_4$	$C_{28}H_{22}F_6MnN_5O_6S_2$
Formula weight ($g\,mol^{-1}$)	637.41	1876.21	1451.14	757.57
Crystal system	Triclinic	Triclinic	Triclinic	Monoclinic
Space group	*P*–1	*P*–1	*P*–1	*C2/c*
a (Å)	7.4133(13)	14.300(5)	11.1874(13)	14.784(2)
b (Å)	12.588(2)	14.624(5)	15.3212(17)	13.917(2)
c (Å)	13.759(2)	18.716(5)	18.595(2)	30.555(5)
α (°)	74.781(2)	95.831(5)	78.6660(10)	
β (°)	79.826(2)	101.049(5)	77.4040(10)	103.000(2)
γ (°)	81.059(2)	112.784(5)	97.649(3)	
Volume ($Å^3$)	1211.5(4)	3474.2(19)	77.4410(10)	6125.8(16)
Z	2	2	2	8
$d_{calcd.}$ ($g\,cm^{-3}$)	1.747	1.794	1.607	1.643
λ (Å)	0.71073	0.71073	0.71073	0.71073
T (K)	100	100	100	100
μ (mm^{-1})	0.814	0.848	0.666	0.656
Reflections collected	6767	16713	14399	15592
Independent reflections	5176 (R_{int} = 0.0135)	12031 (R_{int} = 0.0135)	10386 (R_{int} = 0.0218)	6017 (R_{int} = 0.0232)
F(000)	644	1892	1480	3072
R_1[a], wR_2[b] ($I > 2\sigma(I)$)	0.0308, 0.0858	0.0310, 0.0802	0.0339, 0.0894	0.0353, 0.0880
R_1[a], wR_2[b] (all data)	0.0357, 0.0883	0.0354, 0.0836	0.0383, 0.0925	0.0399, 0.0909
Goodness-of-fit on F^2	1.37	1.027	1.041	1.022
Completeness to θ (%)	93.2	16713	98	99.5
Parameters	355	1143	840	569
Largest diff. peak and hole ($e\,Å^{-3}$)	0.416 and –0.408	0.940 and –0.499	0.554 and –0.474	0.476 and –0.412

[a] $R_1 = \Sigma \, ||F_o| - |F_c|| \, / \, \Sigma \, |F_o|$

[b] $wR_2 = [\, \Sigma \, w(F_o^2 - F_c^2)^2 \, / \, \Sigma \, w(F_o^2)^2 \,]^{1/2}$

References

[1] S.J. Wezenberg, A.W. Kleij, Angew. Chem., Int. Ed. 47 (2008) 2354–2364.

[2] C. Baleizão, H. Garcia, Chem. Rev. 106 (2006) 3987–4043.

[3] (a) V. L. Pecoraro (Ed.), Mangnese Redox Enzymes, VCH, New york, 1992;

(b) P. Rousselot-Pailley, C. Bochot, C. Marchi-Delapierre, A. Jorge-Robin, L. Martin, J. C. Fontecilla-Camps, C. Cavazza, S. Ménage, Chem. Bio. Chem. 10 (2009) 545–552.

[4] (a) G. Bhargavi, M. B. Rajasekharan, J. -P. Costes, J. -P. Tuchagues, Polyhedron, 28 (2009) 1253–1260;

(b) H. Miyasaka, R. Clerac, R. T. Ishii, H. Chang, S. Kitagawa, M. Yamashita, J. Chem., Soc., Dalton Trans. (2002) 1528–1534.

[5] (a) T. Inagaki, T. Mochida, Chem. Lett. 39 (2010) 572–573;

(b) Y. Miura, F. Shimizu, T. Mochida, Inorg. Chem. 49 (2010) 10032–10040;

(c) Y. Funasako, T. Mochida, T. Inagaki, T. Sakurai, H. Ohta, K. Furukawa, T. Nakamura, Chem. Commun. 47 (2011) 4475–4477;

(d) T. Inagaki, T. Mochida, M. Takahashi, C. Kanadani, T. Saito, D. Kuwahara, Chem. Eur. J. doi: 10.1002/chem.201200151.

[6] (a) A. Stark, K.R. Seddon, in Kirk-Othmer Encyclopedia of Chemical Technology, 5th ed.; Kirk-Othmer; Wiley-Interscience, 26 (2007) 836–919;

(b) R.D. Rogers, K.R. Seddon, Eds, Ionic Liquids: Industrial Applications to Green Chemistry; ACS symposium series: Washington DC, 2002;

(c) M. Armand, F. Endres, D.R. MacFarlane, H. Ohno, B. Scrosati, Nature Mater. 8 (2009) 621–629.

[7] P. Bonhôte, A.-P. Dias, N. Papageorgiou, K. Kalyanasundaram, M. Grätzel, Inorg. Chem. 35 (1996) 1168–1178.

[8] (a) K. Miyokawa, T. kawarada, I. Masuda, Thermochim. Acta 83 (1985) 235–241;

(b) K. Miyokawa, M. Itoh, T. Etoh, S. Kinand I. Masuda, Thermochim. Acta 95 (1985) 227–234;

(c) B. Zhou, Y. Zhao, S. Jiang, D. Zhou, Thermochim. Acta 354 (2000) 25–30.

[9] R. Tan, D. Yin, N. Yu, H. Zhao, D. Yin, J. Catal. 263 (2009) 284–291.

[10] A.B. Blake, J.R. Chipperfield, W. Hussain, R. Paschke, E. Sinn, Inorg. Chem. 34 (1995) 1125–

1129.

[11] M. Mikuriya, R. Nukada, W. Tokami, Y. Hashimoto, T. Fujita, Bull. Chem. Soc. Jpn. 69 (1996) 1573–1578.

[12] (a) C. K. Lee, M. J. Ling, I. J. B. Lin, Dalton Trans. 24 (2003) 4731–4737;

(b) C. K. Lee, K.-M. Hsu, C.-H. Tsai, C. K. Lai, I. J. B. Lin, Dalton Trans. 8 (2004) 1120–1126.

[13] (a) T. Akitsu, Y. Takeuchi, Y. Einaga, Acta Cryst. C61 (2005) m324–m328;

(b) Y. Feng, C. Wang, Y. Zhao, J. Li, D. Liao, S. Yan, Q. Wang, Inorg. Chim. Acta 362 (2009) 3563–3568.

[14] (a) P. Coggon, A. T. McPhail, F. E. Mabbs, A. Richards, A.S. Thornley, J. Chem. Soc. A. (1970) 3296–3303;

(b) M.R. Bermejo, M.I. Fernández, E. Gómez-Fórneas, A. González-Noya, M. Maneiro, R. Pedrido, M.J. Rodríguez, Eur. J. Inorg. Chem. (2007) 3789–3797.

(c) A.M. van den Bergen, G.D. Fallon, B.O.West, unpublished result (CSD Refcode: CUBMAN);

[15] H.-L. Shyu, H.-H. Wei., Y. Wang, Inorg. Chim. Acta 290 (1999) 8–13.

[16] M.R. Bermejo, A. Castiñeiras, J.C. Garcia-Monteagudo, M. Rey, A. Sousa, M. Watkinson, C.A. McAuliffe, R.G. Pritchard, R L. Beddoes, J. Chem. Soc., Dalton Trans. (1996) 2935–2944.

[17] A. Garcia-Deibe, M.R. Bermejo, A. Sousa, C.A. McAuliffe, P. McGlynn, P.T. Ndifon, R.G. Pritchard, J. Chem. Soc. Dalton Trans. 10 (1993) 1605–1610.

[18] T. M. Ross, S. M. Neville, D. S. Innes, D. R. Turner, B. Moubaraki, K. S. Murray, Dalton Trans. 39 (2010) 149–159.

[19] M. Okuhata, T. Mochida, in preparation.

[20] J. Dessolin, M. Schuler, A. Quinart, F. De Giorgi, L. Ghosez, F. Ichas, Eur. J. Pharm. 447 (2002) 155–161.

[21] M. Ansarl, S.A.A. Ebrikl, R. Mouhoubl, P. Berthelotl, C. Vaccherl, M.P. Vaccherl, N. Flouquetl, D.H. Caignard, P. Renard, B. Pirard, M.C. Rettor, G. Evrard, F. Durant, M. Debaertl, Eur. J. Med. Chem. 31 (1996) 449–460.

[22] G.M. Sheldrick, Program for the Solution for Crystal Structures; University of Göttingen, Germany, 1997.

[23] G.M. Sheldrick, SADABS. Program for Semi-empirical Absorption Correction, University of Göttingen, Germany, 1996.

[24] ORTEP-3 for Windows: L.J. Farrugia, J. Appl. Cryst. 30 (1997) 565.

TOC